Applied Physics A (2020) 126:941
https://doi.org/10.1007/s00339-020-04124-x

Applied Physics A
Materials Science & Processing

Investigation of the room temperature ferro-magnetism in transition metal-doped ZnO thin films

Arun Kumar[1] · Pooja Dhiman[2] · Sarveena[3] · Sanjeev Aggarwal[1] · Mahavir Singh[3]

Received: 30 July 2020 / Accepted: 2 November 2020 / Published online: 17 November 2020

Abstract
In the present work, we report the ferromagnetic (Fe, Ni) co-doped $Zn_{1-x-y}Ni_yFe_xO$ ($y = 0.01$ and $x = 0.01$, 0.03, 0.05) thin films fabricated through the RF magnetron sputtering on Silicon (400) substrate. Structural studies of prepared thin films through X-ray Diffraction (XRD) reveal the formation of a single-phased hexagonal structure of films. Atomic Force Microscopy (AFM) confirms the decrease in surface roughness with the increase in Fe doping. The optical band gap of the thin films analyzed through the UV–Vis spectroscopy suggests the appropriateness of prepared thin films to be utilized in optoelectronic devices. The magnetic study of these thin films confirmed the room temperature ferromagnetic (RTFM) behavior for prepared thin films. The observed magnetic behavior has been described in view of polaron percolation theory.

Keywords RF magnetron sputtering · X-ray Diffraction (XRD) · Vibrating sample magnetometer (VSM) · Atomic force microscopy (AFM)

1 Introduction

Dilute Magnetic Semiconductor (DMS) in a nanometer size has been widely studied in the past few years, there has been particular interest in correlating their optical, magnetic, and structural properties with the size and shape of the nanostructures [1, 2]. The fabrication of the DMSs thin films having room-temperature ferromagnetism (RTFM) leads to the development of multifunctional spintronic devices [3, 4]. Transition metals, such as Fe, Ni-doped ZnO thin films, were used scientifically in constructive optical, electronic, and magnetic properties essential for spintronic materials [5]. The presence of the room temperature ferromagnetism (RTFM) behavior leads to another dimension towards the multiple applications of the material. The source of magnetism in "un-doped" and "doped" was believed to be powerfully reliant on deformities like Zn interstitials, Oxygen vacancies, and other surface effects [6, 7]. The synthesis route is another important factor that results in varied magnetic character and other properties of diluted magnetic semiconductors which are expected as synthesis procedure may also result in varied defect concentration, vacancies, and morphology, etc. [8]. The cause of presenting RT-FM in the uncontaminated and contaminated semiconductors is still ambiguous. Many reports were supporting the intrinsic magnetism in the diluted magnetic semiconductors and about the defect-induced magnetism. I. Lorite et al. [9] reported that Zn interstitials were primarily dependable for the magnetic ordering in ZnO-based thin films. In contrast, a study by H. Hong et al. [10] revealed that deformity can lead to ferromagnetic behavior or the excess of oxygen could destroy the magnetic arrangements. A few years ago, ZnO-based thin films were fabricated by metal–organic Chemical Vapor Disposition (CVD) technique, Pulsed Laser Deposition (PLD), Sol–Gel, Molecular Beam Epitaxial (MBE), etc. [11–13]. In the middle of these, we make use of the Radio Frequency magnetron sputtering deposition method, which has quite a few benefits, such as thickness, as well as surface roughness has controlled by adjusting the rate of the deposition. RF sputtering has many advantages like low cost, low roughness and it can deposit a wide variety of insulators, metals, alloys, composites, etc. In the present work, we have studied the room temperature ferromagnetism (RTFM) of

✉ Arun Kumar
arunmadeta.phy19@kuk.ac.in

[1] Department of Physics, Kurukshetra University, Kurukshetra, Haryana 136119, India

[2] School of Physics and Material Science, Shoolini University, Solan, H. P 173212, India

[3] Department of Physics, Himachal Pradesh University, Shimla 171005, India

Fe, Ni co-doped ZnO thin films by RF Magnetron sputtering, which have not been reported till now.

2 Experiment

In the experimental part, Synthesis of Dilute Magnetic Semiconductors (DMS) thin films was the same, as we have discussed in our previous article [2]. The Crystal Structure of the Dilute Magnetic Semiconductors thin films was taken in the range of 20º – 80º through X-ray Diffractometer (XRD) (XPERT-PRO diffractometer) with Cu-Kα radiation with the wavelength (λ = 1.54 Å). The (Perkin Elmer Lambda-750) spectrophotometer was used for the optical properties of the thin films with the range of wavelengths 200–800 nm. The NTEGRA-based AFM was used for the surface roughness and surface morphology of the thin films. The Alpha Bruker model carried FTIR studies; Perkin Elmer LS 55 Fluorescence Spectrophotometer carried Photoluminescence study. The thickness of the thin films was measured by the SENTECH Ellipsometer. A "Microsense" Vibrating Sample Magnetometer (VSM) was used for the room temperature magnetic studies with the applied magnetic field of 1 T and the 14TPPMS Vibrating Sample Magnetometer performed the Low-temperature magnetic study with the applied magnetic field of 7 T.

3 Results and discussion

3.1 X-ray diffraction

The X-Ray diffraction arrays of the Ni, Fe co-doped DMS thin films deposited on the Si (400) substrate having the various microscopic element of "dopant" ion $Zn_{1-x-y}Ni_yFe_xO$ ($y = 0.01$, $x = 0.01$, 0.03 and 0.05) and denoted as NZF1, NZF3, NZF5, respectively as shown in Fig. 1 [14].

The crystallite size was calculated from the significant changes in the lattice constant. This indicates that the doped Fe and Ni atoms substitute Zn atoms.

The presence of all the Bragg diffraction in NZF1, NZF3, and NZF5 confirms the formation of the hexagonal wurtzite structure. The diffraction patterns of the thin-film samples were diverse, this represents that the evolution of ZnO in several planes is dissimilar and the evolution is anisotropic. This shows the crystalline nature of transition metal-doped ZnO-based thin films was significantly enhanced through changing the Fe ion with constant Ni concentrations. The

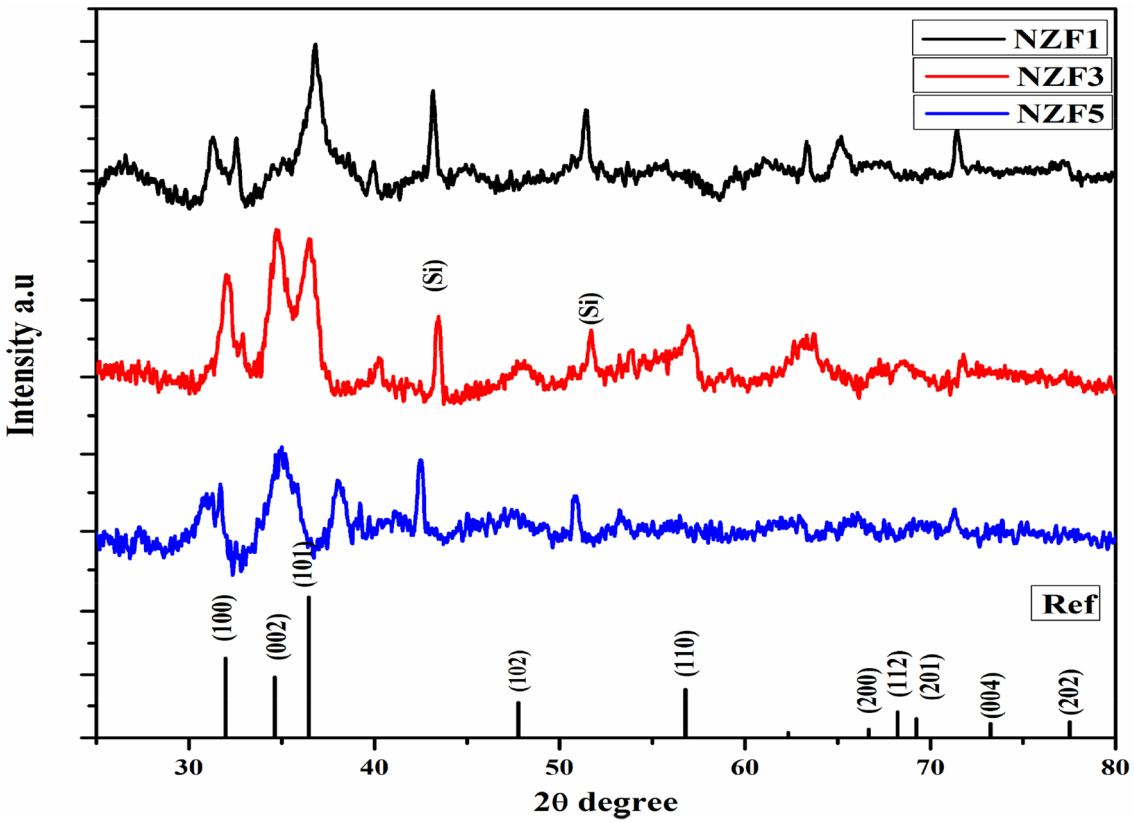

Fig. 1 XRD of $Zn_{1-x-y}Ni_yFe_xO$ ($y = 0.01$, $x = 0.01$, 0.03 and 0.05) thin films

crystalline size of all thin films has been calculated by the Debye–Scherrer formula by considering the most intense peak (002) of each thin film. The Lattice parameter "a" and crystalline size "D" is measured by the relation:

$$D = \frac{k\lambda}{\beta \cos\theta} \tag{1}$$

$$a = \frac{\lambda}{2\sin\theta} \times \sqrt{h^2 + k^2 + l^2} \tag{2}$$

where k (~0.9) is the shape factor, λ is the x-ray wavelength of Cu Kα radiation (λ = 1.54059 Å), β is the full width at half maximum (FWHM), θ is the Bragg diffraction angle of the respective diffraction peak. The larger the half-peak width, the smaller the grain size, i.e. more small grains are produced, indicating that a certain amount of Fe and Ni can inhibit the grain growth of zinc oxide thin films. Then, predictable crystallite sizes were 40, 36, and 30 nm for the thin films NZF1, NZF3, and NZF5, respectively. The particle size decrease with the increase in the Fe concentration, in the whole XRD pattern with the presence of the substrate peaks, marked as Si, no supplementary diffraction peaks not detected. This confirms the "doping" of Fe and Ni was not affecting the original wurtzite geometry of prepared thin films.

3.2 AFM analysis

The average grain size and surface morphology of the thin films have been calculated by AFM analysis. The particles have equally distributed throughout the surface. Overall, the surfaces of all the samples were very smooth. The result shows that doping concentration plays an important role in the surface morphological nature of the thin film. One % of the Fe, Ni co-doped ZnO thin film has the largest surface roughness. The roughness of the thin films decreases, with an increase in Fe concentration. The results also confirm that the morphological variations are maintained by the concentration of Fe, Ni in the film. The variations on the surface roughness were due to the decrease in grain size with a decrease in the absorbency of the films. Linhua Xu [15] reported a similar result earlier. The large surface roughness of the thin films leads to the gas sensor for commercial applications [16].

The AFM works in the non-contact mode (Fig. 2). The relationship between the cantilever's dimensions and spring constant, k, is defined by the equation:

$$k = Ewt^3 / 4L^3 \tag{3}$$

where w = cantilever width; t = cantilever thickness; L = cantilever length and E = Young's modulus of the cantilever

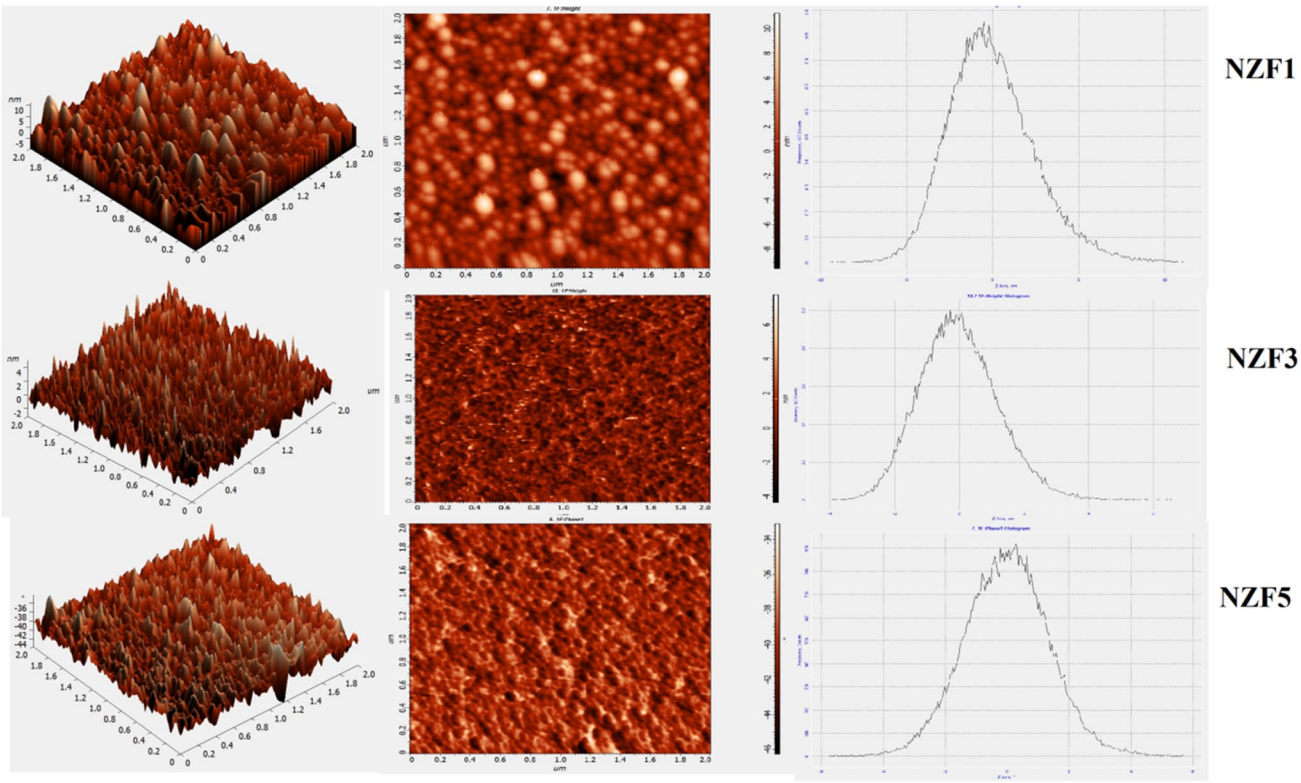

Fig. 2 Surface morphology with the histogram of $Zn_{1-x-y}Ni_yFe_xO$ ($y = 0.01$ and $x = 0.01$, 0.03 and 0.05) thin films

material. The natural frequency (ω_0) of a cantilever is related to its spring constant (k) and mass (m) [17].

$$\omega_0 = \sqrt{k/m} \tag{4}$$

Figure 2 shows two-dimensional (2D) AFM surface height morphologies of Fe, Ni co-doped ZnO thin-film scanning area with a dimension of $2\times2\mu m^2$. The 3D replicated morphology of the thin film describes the growth along the C-axis and this result resembles the preferred (002) plane orientation through X-ray diffraction results. In the present study, the decrease in grain size also due to the micro-densification effect. In that case, the number of nuclei of metal increases as an effect of increasing precursor concentration [18], which leads to the formation of a denser and compact structure of the ZnO thin film on the substrate surface. The low surface Ni-doped thin film is also used as a NO_2 Sensor [19].

3.3 Ellipsometry study

Ellipsometry study is an important thin-film measurement technology for its non-destructive, non-contact, and delicate advantages. The thickness of the thin films was measured by an ellipsometer with a wavelength of 632.8 nm. The thickness of the thin films was found to be around 133.65 nm. An optical model was used for the surface thickness of the thin film. The optical model for the analysis is conventional as follows: Sisubstrate/doped ZnO thin-film layer/surface roughness/air ambient, as shown in Fig. 3.

3.4 Optical studies

Figure 4a shows the optical absorbance properties of the Zn_{1-x-y} Ni_yFe_xO ($y=0.01$, $x=0.01$, 0.03 and 0.05) thin films deposited on Si (400) substrate. The Tauc's plot was used for calculation of the energy "bandgap" Eg of the prepared thin films. The absorption spectrum of DMS thin films shows sinusoidal behavior, which is due to, the covered structure of thin films. ZnO is a direct band transitions material and the absorption coefficient, which has been denoted by α expressed by the Eq. (5)

$$\alpha hv = A\,(hv - E_g)^r \tag{5}$$

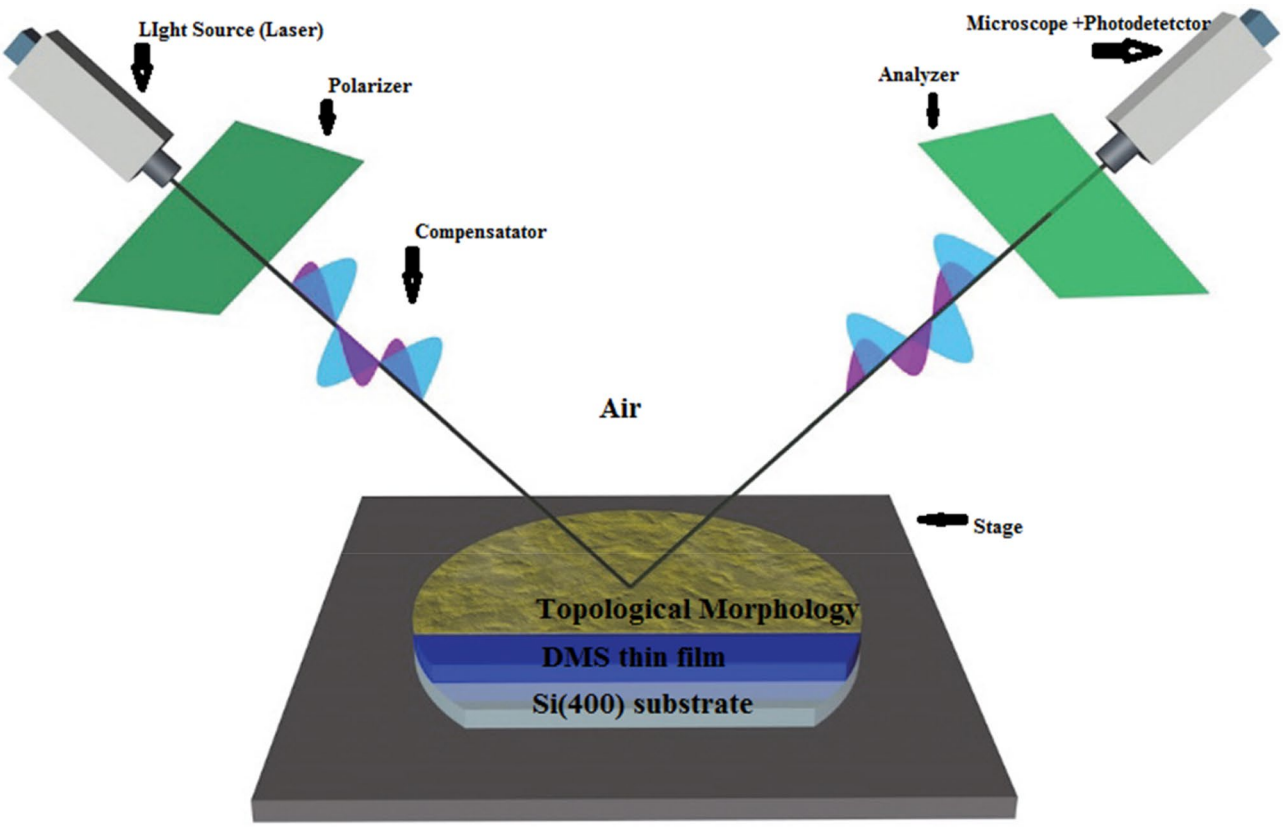

Fig. 3 Spectroscopic ellipsometer schematic micro nanosystems of a Fe–Ni co-doped thin film

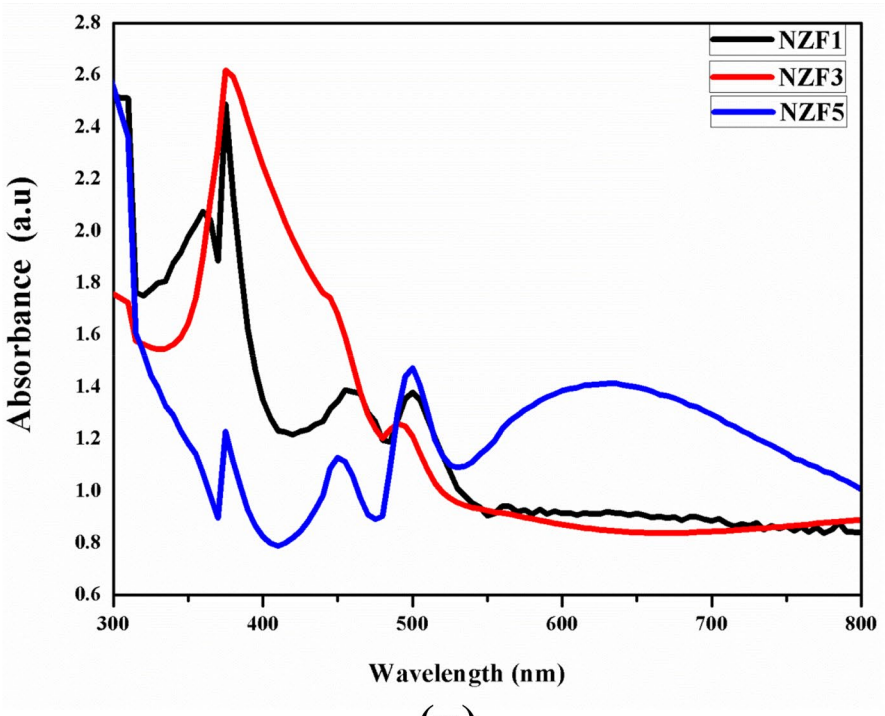

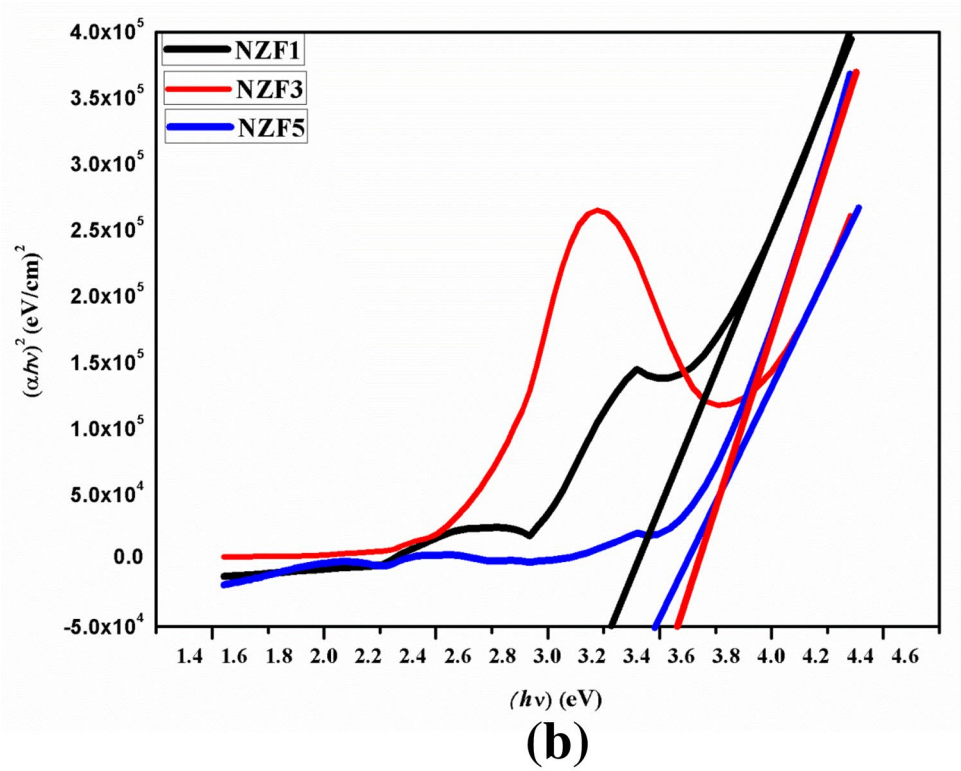

Fig. 4 **a** The UV–Vis spectraof the Zn_{1-x-y} Ni_yFe_xO ($y=0.01$, $x=0.01$, 0.03 and 0.05)thin films. **b**The energy band gap of the Zn_{1-x-y} Ni_yFe_xO ($y=0.01$, $x=0.01$, 0.03 and 0.05)thin films

where A is the constant, Eg is the allowed energy gap, hν is the photon energy. In our case, we have direct band transition so the value of $r=1/2$.

Figure 4b shows the absorption coefficient (α) and the two defined regions separated by the peak of the derivative of the absorption coefficient. Te Urbach's area shows the

structural and thermal chaos present in the thin film. The occurrence of an only incline in the plot indicates that the thin films have directed an acceptable transition. The tangent was taken by considering a common point for both the axis and extrapolating the $(\alpha h\nu)=0$, the straight-line portion of the plot to zero absorption coefficient. The band gap E_g of thin films varies from 2.6 to 3.5 eV. The cause for the enhancement in the bandgap is a blue shift, which arises due to the Moss–Burstein band-filling result in which the Fermi level lies in the conduction band [14, 20]. This variation in the "bandgap" is due to the "quantum confinement" of the nano-crystal.

3.5 Photoluminesence (PL) study

Photoluminescence (PL) spectroscopy is an important tool to characterize the optical properties of dilute magnetic semiconductors. The intensity of the Photoluminescence spectrum varies directly to the imperfection concentration present in the fluorescent material. It was apparent that all ZnO thin films with various Fe and Ni co-doping concentrations revealed one violet emission peak with a wavelength of about 338 nm; moreover, emission peak also found. The absence of extra emission peaks is an indication of less number of defects in the thin films.

Figure 5 shows the room temperature Photoluminescence spectrum of different ZnO thin films with various concentrations of Fe and Ni co-dopant. A comprehensible decrease in the intensity of this band is seen in the sample NZF3 in contrast with NZF1 and NZF5 indicating the successful assimilation of the dopants in the ZnO matrix. The slight change in the peak site is also observed in the spectrum, and the shift can be attributed to the change in the band-gap of thin films [21].

3.6 Ftir study

FTIR spectroscopy provides information regarding the functional groups, types of molecular interactions present in the compounds. We have employed FTIR spectroscopy to collect vibrational bands' information and to study the vibrational level changes after the addition of the dopants. The FTIR spectrums for prepared thin films have been presented in Fig. 6.

The absorption peak at 1100 cm^{-1} indicates the sulphate group present in the material [22], which approves the outcomes from XRD. The peak at 484 cm^{-1} in all the spectra gave the Zn–O vibration while the peak at 614 cm^{-1}, found for Fe-doped materials are characteristic of a Fe–O stretch [23, 24]. So that we consider that Fe ions were replaced by Zn ions and fused into the crystal lattice of ZnO.

3.7 Magnetic properties

To explore the magnetic properties of prepared thin films, hysteresis curves were recorded using a Vibrating Sample Magnetometer (VSM). Figure 7a presents the room temperature hysteresis curve for Zn1-x-yNiyFexO ($y=0.01$, $x=0.01$, 0.03 and 0.05) films measured under a magnetic field up to 1 T. It can be seen from the curve that they exhibit room-temperature ferromagnetism. Here, few probable descriptions for RT saturated the hysteresis loop. One is extrinsic was found by P.Dhiman et al. and another one is intrinsic magnetism by D. Karmakar et al. [25, 26]. However, XRD

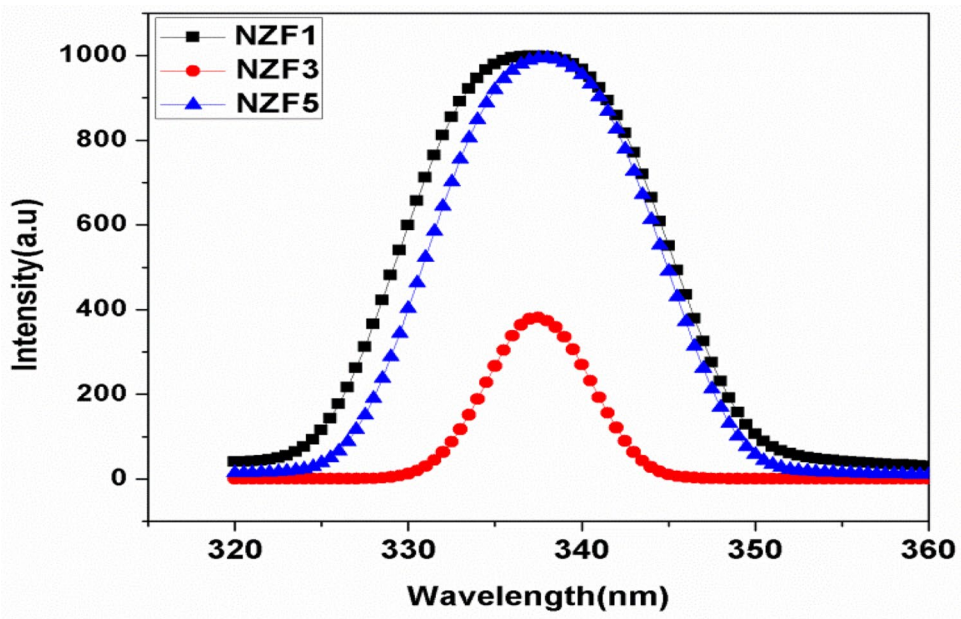

Fig. 5 PL Spectra of $Zn_{1-x-y}Ni_yFe_xO$ ($y=0.01$, $x=0.01$, 0.03 and 0.05) thin films

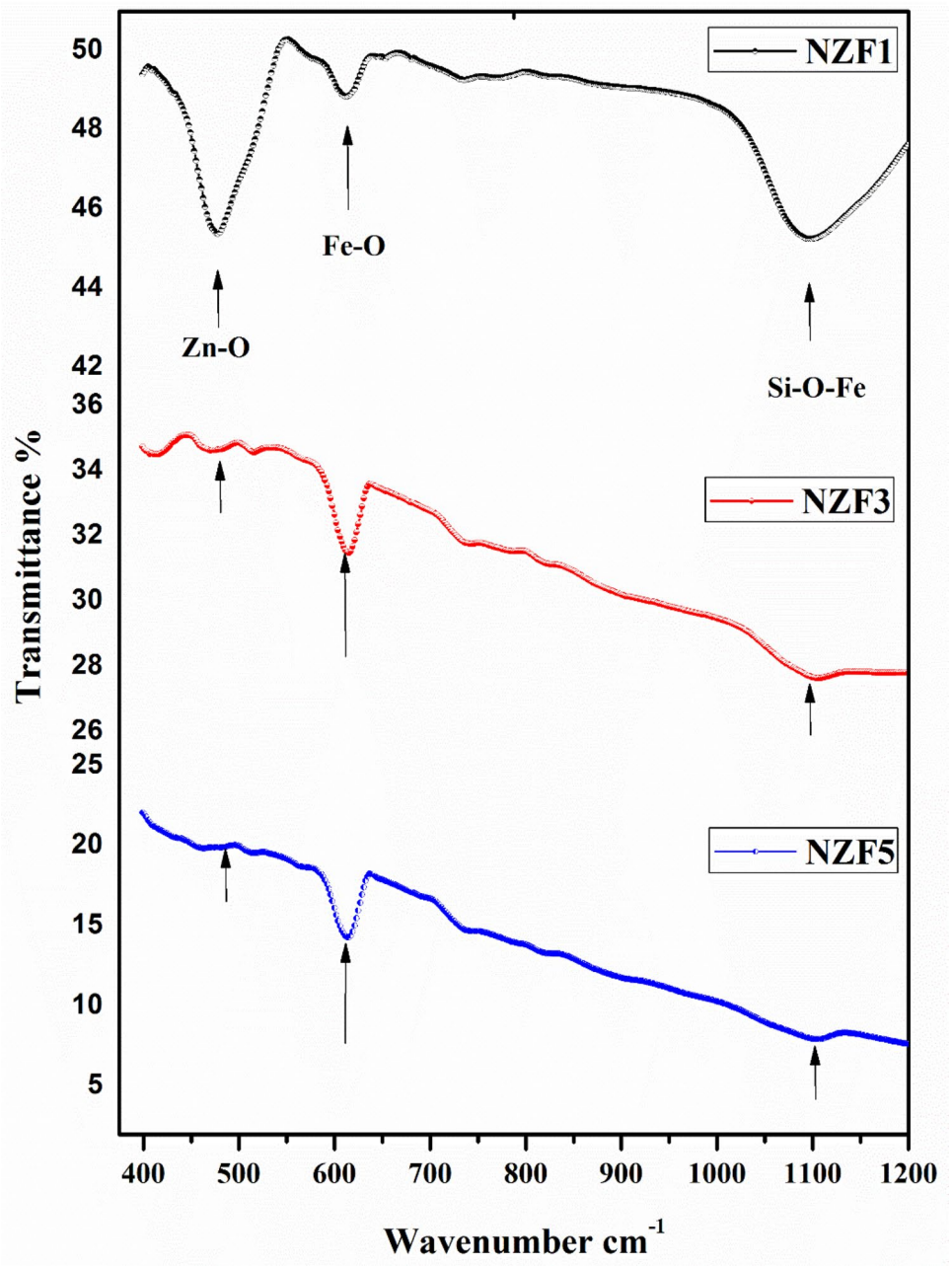

Fig. 6 FTIR Spectra of $Zn_{1-x-y}Ni_yFe_xO$ ($y=0.01$, $x=0.01$, 0.03 and 0.05)thin films

has revealed the absence of any type of impurity or clusters present in the thin films. There is a decrease in the magnetization with the increase in the Fe concentration at the fixed Ni concentration in the thin films. This is clear evidence that merely, Ni and Fe or Ni, Fe clusters have not contributed to the RT-FM behavior of the prepared thin films. Therefore, it was a high possibility of existing several interaction mechanisms between Ni and Fe spins, which have resulted in room temperature ferromagnetism. Recently, reported work on Ni-doped ZnO thin films deposited through spray pyrolysis method revealed a similar type of room temperature results but low-temperature hysteresis loops were unsaturated even under application of 50 kOe [27]. In other findings of Fe-doped ZnO thin films fabricated through the sol–gel spin coating technique, saturation magnetization was found to be below 11 emu/g for 20 at.% Fe doping [28].

We have also recorded M-H curves for thin films at 5 K (Fig. 7b), which also shows the ferromagnetic nature of the samples with increased and saturated magnetization values. To further, explore the exact cause of RTFM, low-temperature magnetic studies are done. Field cooled (FC) and zero fields cooled (ZFC) measurements are performed at 5 K and the observed values of magnetization and coercivity are presented in Table 1 (Fig. 8).

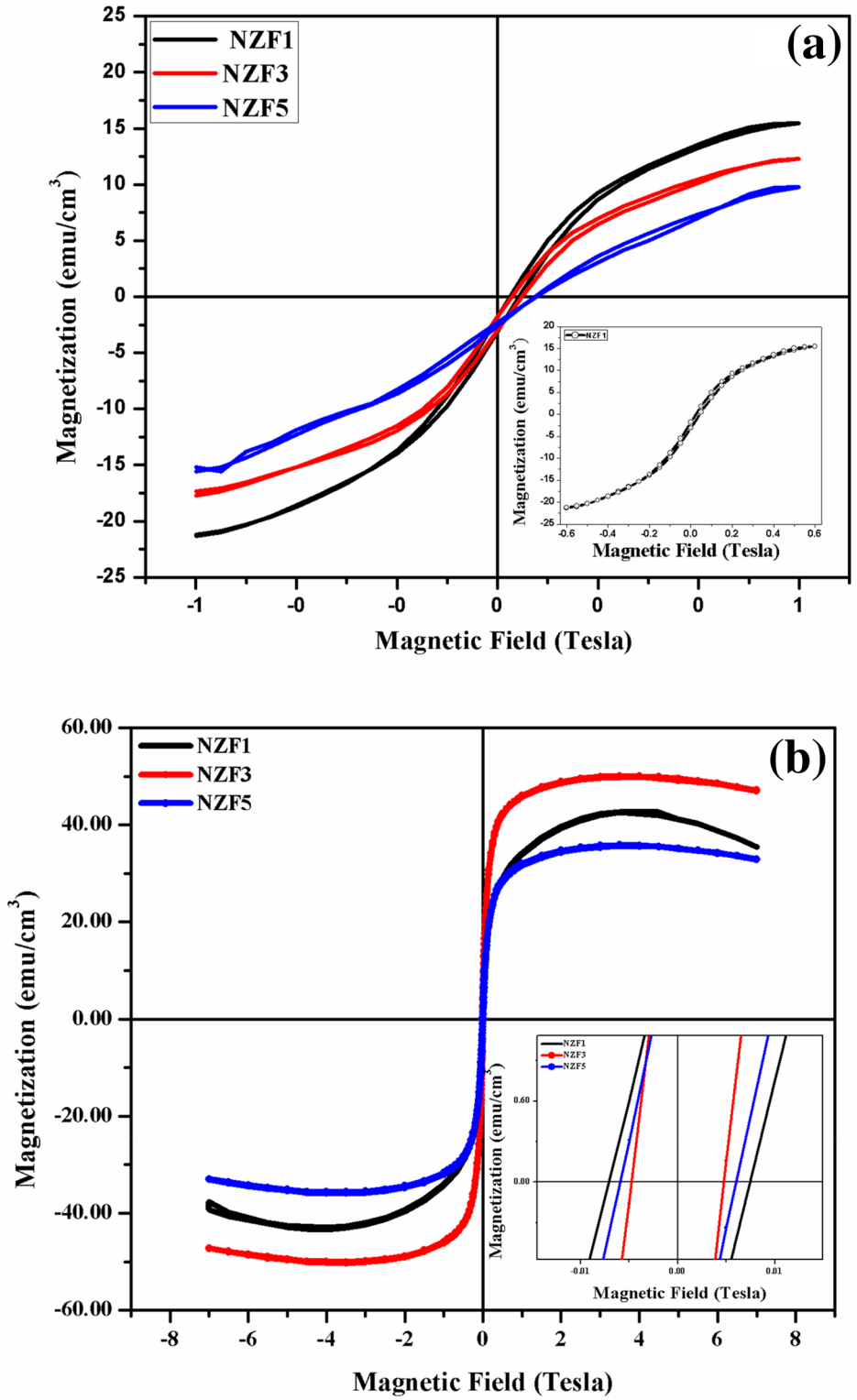

Fig. 7 **a**The magnetic hysteresis loops of the $Zn_{1-x-y}Ni_yFe_xO$ ($y=0.01$, $x=0.01$, 0.03 and 0.05) thin films at 300 K, **b** at 5 K

Figure 8 shows FC-ZFC curves of $Fe_{0.01}$- and $Ni_{0.01}$-doped ZnO thin films taken from 5 to 300 K. ZFC curve was found by primarily cooling the thin films from 300 to 5 K in the nonappearance of an applied magnetic field and warming up in 7 T field during the magnetization measurement. Both the FC mode and ZFC mode curves present unique behavior at very low temperatures. The FC curve shows a decrease in magnetization with an increase in temperature. However, the

Table 1 The observed magnetization and coercivity at 5K temperatures are given in table

Sample Zn_{1-x-y} Ni_yFe_xO	M (emu/cm^3)	H_c (Oe)
y=0.01, x=0.01	34.24	0.0075
y=0.01, x=0.03	54.63	0.0047
y=0.1, x=0.05	37.45	0.0061

decrease is very prominent at low temperatures. However, by analyzing the ZFC curve, we found that they are not blocking temperature that exists below 300 K.

Both FC and ZFC start following the same behavior after 290 K. However, as there is a clear separation between the FC–ZFC curves close to room temperature, which implies the ferromagnetic behavior of the samples close to room temperature. The experimental values of the magnetron number have been estimated by employing the following relation:

$$n_{(B)}^{N} = \frac{(\text{Sat.Magnetization} \times \text{Mol.weight})}{5585} \tag{6}$$

The theoretical values of the magnetron number have been estimated in the light of Neel's two sublattice model [29]:

$$n_{(B)}^{N} = \text{MB (X)} - \text{MA (X)} \tag{7}$$

where the symbols have their usual meanings. The cause of ferromagnetism may be attributed to the different mechanisms suggested by various authors [30–33], including bound magnetic polaron theory, defect-induced, magnetism, carrier-mediated and RKKY interactions, etc. by going through the previous reports, the curve of magnetization vs. temperature was detected in a carrier-localized regime, which can be explained by the polaron percolation theory [34].

Along with this concept, the polaron percolation threshold (δ_p) and the cation percolation threshold (x_p) were the two main milestones which contribute to the magnetic phase diagram. If we have a large number of the magnetic cations in the samples, then the ferromagnetic nature has been observed by satisfying the condition $\delta < \delta_p$ and $x < x_p$. In the case of cation threshold $x < x_p$, then the long-range ordering cannot lead to the anti-ferromagnetic superexchange interaction in the material. Now, by the concept of percolation theory, the distance between polaron–polaron is large enough for the generation of the strong ferromagnetic ordering. From all the characterizations, we can summarize that the detected RT-FM is not due to the defects or some other phase formation but only is the intrinsic one. To further explore the materials under study, simulations can be performed for microstructural analysis [35, 36]. In the future, to study the effects of synthesis techniques used for preparing target for sputtering techniques, other synthesis routes can be opted [37–39].

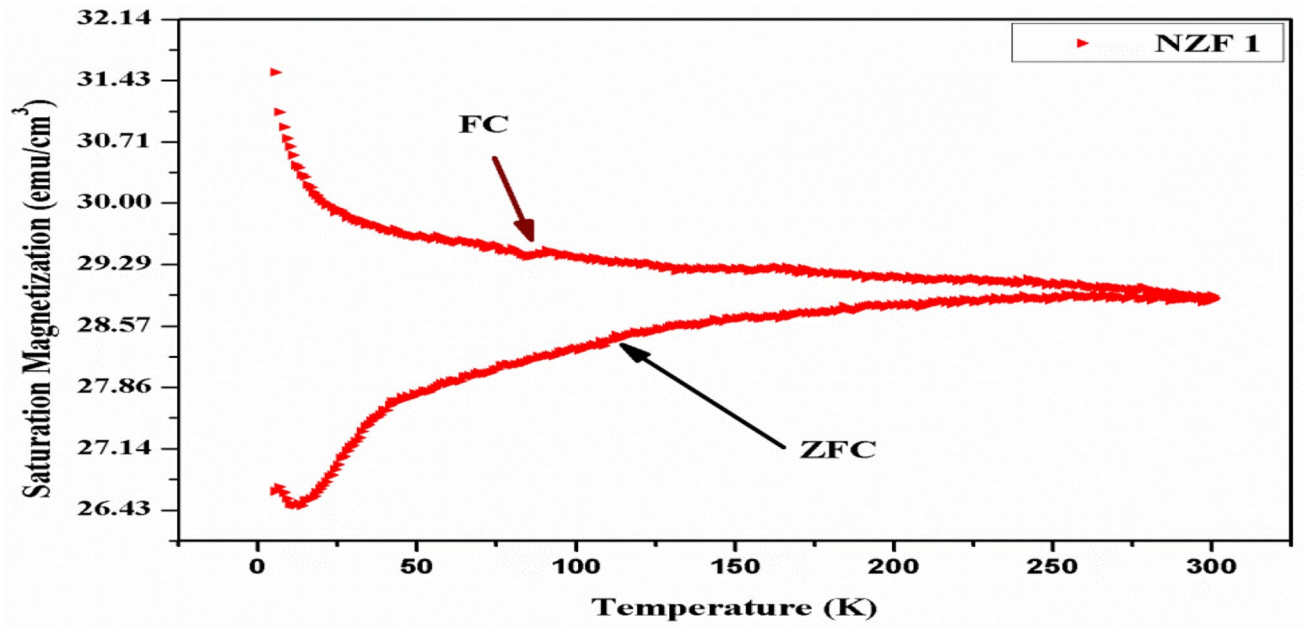

Fig. 8 FC (Field-Cooled) and ZFC (Zero Field-Cooled) thermal variations of the saturation magnetization for NZF1 thin film under a magnetic field H = 7KOe

4 Conclusion

In conclusion, Fe, Ni co-doped thin films successfully deposited on Silicon (400) substrate shows noticeable ferromagnetism at the room as well as at low temperatures. XRD revealed that there are no other impurities present in the thin film. The surface roughness of the prepared thin films reduced with the increment in Fe, Ni contents, which were explained by the micro-densification effect. Our X-ray diffraction studies are also supported by the AFM data analysis of the thin film. The variation of optical band gap energy on the carrier density is explained by the Moss–Burstein effect and quantum confinement. Magnetic studies reveal the room temperature ferromagnetism in the thin film. Observed intrinsic RTFM and optical results make these thin films suitable for spintronic applications and optoelectronic devices.

Acknowledgements Dr. Arun Kumar would like to thank the Department of Science and Technology (DST) for the Research Associate Fellowship under the project no SR/MF/PS/-05/2017/G. The author also likes to thank the UGC-DAE consortium Indore for the low-temperature magnetic study.

References

1. C. Liu et al., J. Magn. Magn. Mater. **324**(20), 3356–3360 (2012)
2. A. Kumar, P. Dhiman, M. Singh, Ceram. Int. **42**(7), 7918–7923 (2016)
3. P. Sharma, Science **307**(5709), 531–533 (2005)
4. S. Pearton, C. Abernathy, D. Norton, A.F. He Bard, Y.D. Park, L.A. Boatner, J.D. Budai, Mater. Sci. Eng. R. **40**, 137 (2003)
5. S. Yılmaz et al., Chem. Phys. Lett. **525**, 72–76 (2012)
6. Q. Xu, C. Grudmann, M. Meinecke et al., Appl Phys Lett **92**, 082508 (2008)
7. P. Satyarthi et al., J. Appl. Phys. **113**(18), 183708 (2013)
8. P. Dhiman et al., Micro. Nano. Lett. **7**, 1333–1335 (2012)
9. I. Lorite et al., Appl. Phys. Lett. **106**(8), 082406 (2015)
10. N.H. Hong et al., Phys. Rev. B **72**(4), 045336 (2005)
11. H. Liu et al., J. Phys. Condens. Matter **21**(14), 145803 (2009)
12. C. Prajapati, A. Kushwaha, P. Sahay, J. Therm. Spray Technol. **22**(7), 1230–1241 (2013)
13. B. Ghosh et al., J. Appl. Phys. **123**(16), 161507 (2018)
14. M. Feneberg et al., Phys. Rev. B. **90**(7), 075203 (2014)
15. D. Fang et al., J. Alloy. Compd. **589**, 346–352 (2014)
16. R. Kumaravel et al., Nucl. Instrum. Methods Phys. Res. Sect. B **268**(15), 2391–2394 (2010)
17. M.K. Dounkal, R. Bhan, Sens. Transduc. **228**(12), 84–86 (2018)
18. V. Shinde, T. Gujar, C. Lokhande, Sens. Act. B. Chem. **120**(2), 551–559 (2007)
19. S. Jain et al., Mater. Sci. Eng. B **247**, 114381 (2019)
20. P. Dhiman et al., J. Alloy. Compd. **578**, 235–241 (2013)
21. A. Kumar, P. Dhiman, S. Aggarwal, M. Singh, Res. Square (2020). https://doi.org/10.21203/rs.3.rs-44212/v1
22. A. Chelouche, D. Djouadi, A. Aksas, Eur. Phys. J. Appl. Phys. **64**(1), 10304 (2013)
23. R. Fu et al., Mater. Lett. **62**(25), 4066–4068 (2008)
24. R. Hong et al., Mater. Res. Bull. **43**(8–9), 2457–2468 (2008)
25. P. Dhiman et al., Appl. Surf. Sci. **287**, 287–292 (2013)
26. R.M. K.D.M.S.K., T.K. P.P.R.A.N., A.K. Das, I. Dasgupta, G.P. Das, Phys. Rev. B. **75**, 144404 (2007)
27. H. Ali et al., J. Alloy. Compd. **816**, 152538 (2020)
28. P. Ariyakkani, L. Suganya, B. Sundaresan, J. Alloy. Compd. **695**, 3467–3475 (2017)
29. G. Kumar et al., Phys. Chem. Chem. Phys. **19**(25), 16669–16680 (2017)
30. D. Mukherjee et al., Phys. Rev. B **81**(20), 205202 (2010)
31. A. Samariya et al., Mater. Chem. Phys. **123**(2–3), 678–684 (2010)
32. M. Venkatesan et al., Phys. Rev. Lett. **93**(17), 177206 (2004)
33. A. Kocyigit, R. Topkaya, Mater. Res. Exp. **6**(9), 096116 (2019)
34. A. Kaminski, S.D. Sarma, Phys. Rev. Lett. **88**(24), 247202 (2002)
35. A.M. Roy, JETP. Lett. **112**(3), 173–179 (2020)
36. A.M. Roy, Appl. Phys. A **126**(7), 1–12 (2020)
37. S. Mortazavi-Derazkola, S. Zinatloo-Ajabshir, M. Salavati-Niasari, Ceram. Int. **41**(8), 9593–9601 (2015)
38. S. Ahmadian-Fard-Fini et al., Carbohyd. Polym. **229**, 115428 (2020)
39. M. Salavati-Niasari, F. Davar, M. Mazaheri, J. Alloy. Compd. **470**(1–2), 502–506 (2009)